

## Pulse-Gated Quantum-Dot Hybrid Qubit

Teck Seng Koh, John King Gamble, Mark Friesen, M. A. Eriksson, and S. N. Coppersmith

*Department of Physics, University of Wisconsin-Madison, Madison, Wisconsin 53706, USA*

(Received 24 July 2012; published 20 December 2012)

A quantum-dot hybrid qubit formed from three electrons in a double quantum dot has the potential for great speed, due to the presence of level crossings where the qubit becomes chargelike. Here, we show how to exploit the level crossings to implement fast pulsed gating. We develop one- and two-qubit dc quantum gates that are simpler than the previously proposed ac gates. We obtain closed-form solutions for the control sequences and show that the gates are fast (subnanosecond) and can achieve high fidelities.

DOI: [10.1103/PhysRevLett.109.250503](https://doi.org/10.1103/PhysRevLett.109.250503)

PACS numbers: 03.67.Lx, 73.21.La, 85.35.Be

A key figure of merit for a quantum information processing device is the ratio of the quantum coherence time to the time required to perform qubit gate manipulations [1–3]. The recently proposed hybrid quantum dot qubit [4] is a relatively simple qubit architecture that could achieve a higher figure of merit [5] than previous qubit designs [6–8]. The qubit itself is a set of two states of three electrons in a (2,1) charge configuration with total spin quantum numbers  $S^2 = 3/4$  ( $S = 1/2$ ) and  $S_z = -1/2$ , with the two different states using the singlet and triplet in a doubly occupied dot and a single spin in a singly occupied dot. In a Heitler-London description of the doubly occupied dot, in the singlet state, both electrons are in the lowest-energy orbital, while in the triplet state, one electron is in an excited orbital, so the two qubit states have different energies. Reference [4] proposes to implement gate operations using high-frequency ( $\sim 10$ – $40$  GHz) resonant rf pulses, which is feasible [9,10], but significantly more complicated to implement experimentally than the pulse-gating methods used for charge qubits [11–15] and for spin qubits [16–20]. Here we show how to implement pulse gating of the quantum dot hybrid qubit. One- and two-qubit gates require a modest number of nonadiabatic voltage pulses (five and eight, respectively).

The two logical qubit states of the quantum-dot hybrid qubit are  $|0\rangle_L = |S\rangle|\downarrow\rangle$  and  $|1\rangle_L = \sqrt{1/3}|T_0\rangle|\downarrow\rangle - \sqrt{2/3}|T_-\rangle|\uparrow\rangle$ , where  $|S\rangle$ ,  $|T_-\rangle$ , and  $|T_0\rangle$  are two-particle singlet ( $S$ ) and triplet ( $T$ ) states in the left dot, and  $|\uparrow\rangle$  and  $|\downarrow\rangle$  respectively denote a spin-up and spin-down electron in the right dot. The hybrid qubit has the same symmetries in spin space as the triple-dot qubit proposed in Ref. [8], but is simpler to fabricate because it uses a double dot instead of a triple dot. Transitions between the logical states  $|0\rangle_L$  and  $|1\rangle_L$  are allowed when tunneling is introduced between the dots. Transitions between  $|0\rangle_L$  and  $|1\rangle_L$  occur via an intermediate state  $|E\rangle$  that has charge occupation (1,2) and the same total  $S^2$  and  $S_z$ . Figure 1(a) shows the hybrid qubit and a physical process that yields transitions between  $|0\rangle_L$  and  $|1\rangle_L$ . We assume that the right dot's singlet-triplet splitting is large enough that higher energy states of the right dot do not mix appreciably with the states considered explicitly here.

Quantum oscillations between two states  $|\alpha\rangle$  and  $|\beta\rangle$  are achieved by changing the detuning suddenly to a value at which the energy difference between the states is smaller than the coupling between them. Very near the avoided crossing between two states, the time evolution is governed by the two-state Hamiltonian

$$H = \begin{pmatrix} \tilde{\varepsilon}/2 & \Delta \\ \Delta & -\tilde{\varepsilon}/2 \end{pmatrix}, \quad (1)$$

where  $\Delta$  is the coupling between  $|\alpha\rangle$  and  $|\beta\rangle$  and  $\tilde{\varepsilon}$  is the energy difference between  $|\alpha\rangle$  and  $|\beta\rangle$  in the absence of coupling. Significant mixing between the states occurs only when  $\tilde{\varepsilon} \lesssim \Delta$ . If one pulses the system suddenly to  $\tilde{\varepsilon} = 0$ , so that the state at time  $t = 0$  is  $|\psi(0)\rangle = |\alpha\rangle$ , then the time evolution of the two-state system is given by  $|\psi(t)\rangle = \cos(\Omega_R t)|\alpha\rangle - i \sin(\Omega_R t)|\beta\rangle$ , oscillating between  $|\alpha\rangle$  and  $|\beta\rangle$  with angular frequency  $\Omega_R = \Delta/\hbar$ . A pulse of duration  $T$  rotates the state on the Bloch sphere by an angle  $\Theta = 2\Omega_R T$  around the  $x$  axis [21].

Figure 1(b) shows the energies of the states  $|0\rangle_L$ ,  $|1\rangle_L$ , and  $|E\rangle$  as a function of detuning  $\varepsilon$ , which is controlled using gate voltages. The energy difference between  $|0\rangle_L$  and  $|1\rangle_L$ , which is the singlet-triplet energy splitting in the left dot, typically is substantial ( $\sim 0.1$  meV, corresponding to a frequency  $\sim 25$  GHz) and depends only moderately on  $\varepsilon$  [22], so achieving an avoided crossing of  $|0\rangle_L$  and  $|1\rangle_L$  is typically not feasible. Therefore, pulse gating is ineffective in inducing transitions directly between  $|0\rangle_L$  and  $|1\rangle_L$ . However, there is a detuning  $\varepsilon_A$  where there is an avoided crossing between the states  $|E\rangle$  and  $|0\rangle_L$  [23], and another detuning  $\varepsilon_B$  where there is an avoided crossing between the states  $|E\rangle$  and  $|1\rangle_L$ . Transitions from  $|0\rangle_L$  to  $|1\rangle_L$  can be induced by pulsing first to  $\varepsilon_A$  and then to  $\varepsilon_B$ . Similarly, transitions from  $|1\rangle_L$  to  $|0\rangle_L$  can be induced by pulsing first to  $\varepsilon_B$  and then to  $\varepsilon_A$ .

*Arbitrary single-qubit rotations.*—A pulse sequence that implements  $U(\hat{\mathbf{n}}, \beta)$ , a rotation of the logical qubit by an angle  $\beta$  about the rotation axis  $\hat{\mathbf{n}} = (\sin\eta \cos\zeta, \sin\eta \sin\zeta, \cos\eta)$ , where  $\eta$  and  $\zeta$  are the polar and azimuthal angles, is constructed from three primitive gates:  $A$ ,  $B$ , and  $P$ . All detuning changes are assumed to be instantaneous. The  $B$  gate,

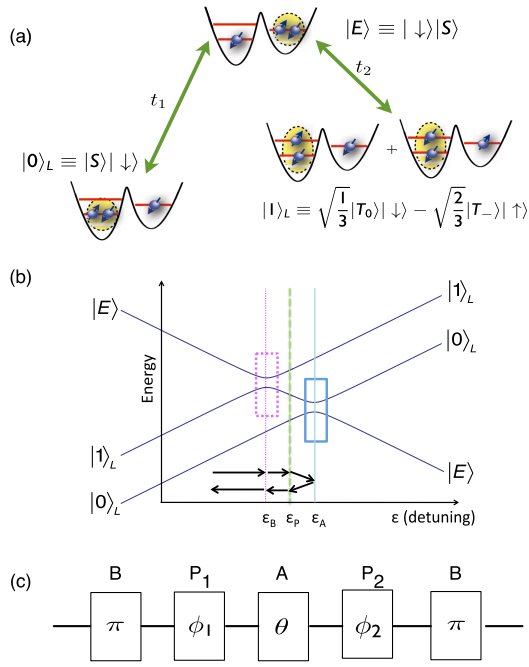


FIG. 1 (color online). (a) Schematic of the quantum-dot hybrid qubit and of the physics underlying gate operations. The logical qubit states are  $|0\rangle_L \equiv |S\rangle|\downarrow\rangle$  and  $|1\rangle_L \equiv \frac{1}{\sqrt{3}}|T_0\rangle|\downarrow\rangle - \sqrt{\frac{2}{3}}|T_-\rangle|\uparrow\rangle$ , where  $|S\rangle$ ,  $|T_-\rangle$ , and  $|T_0\rangle$  are two-particle singlet ( $S$ ) and triplet ( $T$ ) states in the left dot, and  $|\uparrow\rangle$  ( $|\downarrow\rangle$ ) denotes a spin-up (spin-down) electron in the right dot. Introducing tunneling amplitudes  $t_1$  and  $t_2$  to a (1,2) excited state  $|E\rangle$  induces transitions between  $|0\rangle_L$  and  $|1\rangle_L$ . (b) Energies of  $|0\rangle_L$ ,  $|1\rangle_L$ , and  $|E\rangle$  versus detuning  $\varepsilon$  between the two dots. The ground state has charge occupation (2,1) when  $\varepsilon < \varepsilon_A$  and (1,2) when  $\varepsilon > \varepsilon_A$ ; the qubit operates mainly in the regime  $\varepsilon \leq \varepsilon_A$ . The energy difference between the qubit states  $|0\rangle_L$  and  $|1\rangle_L$  is large for all values of  $\varepsilon$ , but there is an avoided crossing between  $|0\rangle_L$  and  $|E\rangle$  at detuning  $\varepsilon_A$  (blue box), and another avoided crossing between  $|1\rangle_L$  and  $|E\rangle$  at  $\varepsilon_B$  (dotted magenta box). Pulse-gate transitions between  $|0\rangle_L$  and  $|1\rangle_L$  can be performed by using both avoided crossings. Pulses to the detuning  $\varepsilon_P$  are used to induce phase differences between the three states. A gating sequence to perform arbitrary rotations in the qubit Hilbert space is indicated with arrows; along the detuning axis, the pulse sequence is  $\varepsilon_i \rightarrow \varepsilon_B \rightarrow \varepsilon_P \rightarrow \varepsilon_A \rightarrow \varepsilon_P \rightarrow \varepsilon_B \rightarrow \varepsilon_f$ . (c) The corresponding circuit diagram for the gate sequence, with time progressing from left to right. Gates  $P_1$ ,  $A$ , and  $P_2$  are tunable, with the control parameters  $\phi_1$ ,  $\theta$ , and  $\phi_2$  given in Eqs. (2)–(4).

implemented by pulsing the detuning to  $\varepsilon_B$  for a time that yields a  $\pi$  rotation about the  $x$  axis in the  $\{|1\rangle_L, |E\rangle\}$  subspace, converts  $|1\rangle_L \rightarrow |E\rangle$  and  $|E\rangle \rightarrow |1\rangle_L$ . The  $A$  gate, obtained by pulsing to  $\varepsilon_A$  for an interval that implements a rotation by an arbitrary angle  $\theta$  about the  $x$  axis in the  $\{|0\rangle_L, |E\rangle\}$  subspace, changes the “latitude” of the qubit on the  $\{|0\rangle_L, |E\rangle\}$  Bloch sphere. The “longitude” on the  $\{|0\rangle_L, |E\rangle\}$  Bloch sphere is controlled using a phase gate  $P$ , whose detuning  $\varepsilon_P$  is roughly midway between the anti-crossings at  $\varepsilon_A$  and  $\varepsilon_B$ , to avoid causing quantum oscillations. The  $P$  gate causes  $|E\rangle$  to gain phase  $\phi$  relative to  $|0\rangle_L$ .

By inserting two  $P$  gates that rotate the phase by angles  $\phi_1$  and  $\phi_2$  between the  $B$  and  $A$  gates, any prescribed rotation on the  $\{|0\rangle_L, |1\rangle_L\}$  Bloch sphere can be obtained. The full pulse sequence  $U = BP_2AP_1B$  is shown at the bottom of Fig. 1(b) and as a circuit diagram in Fig. 1(c). The control parameters  $(\theta, \phi_1, \phi_2)$  that yield rotation parameters  $(\beta, \eta, \zeta)$  are [24]

$$\theta = 2 \arcsin[\sin(\eta) \sin(\beta/2)], \quad (2)$$

$$\phi_1 = \arctan[\cos(\eta) \tan(\beta/2)] - \phi_B - \zeta + \pi/2, \quad (3)$$

$$\phi_2 = \arctan[\cos(\eta) \tan(\beta/2)] - \phi_B + \zeta + \pi/2, \quad (4)$$

where  $\phi_B$  is the incidental phase gained by state  $|1\rangle$  relative to  $|0\rangle$  while implementing the  $B$  gate. For example,  $U = BP_2(-\phi_B + \pi/2)A(\beta)P_1(-\phi_B + \pi/2)B$  yields an  $X$ -rotation by an angle  $\beta$ .

The speed of a pulsed gate in a quantum-dot hybrid qubit can be estimated by noting that it is composed of five primitive gates, as shown in Fig. 1(c). The  $A$  and  $B$  gates correspond to charge qubit rotations, and their speed is determined by the anti-crossing energy gaps [5,11,12,14,15,25]. A  $\pi/2$  rotation of a charge qubit can be implemented in a time  $\leq 200$  ps [5,15]. The speed of the phase gates  $P_1$  and  $P_2$  is determined by the energy splitting between states  $|0\rangle$  and  $|E\rangle$ . For a splitting of  $50 \mu\text{eV}$ , a single  $P$  gate can be implemented in  $\leq 80$  ps. Thus, subnanosecond gating of a hybrid qubit should be achievable with current technology. Subnanosecond coherent driven oscillations between the (2,1) singlet and both of the low energy (1,2) states in a Si/SiGe double dot have been reported [5], providing further evidence that fast pulse-gating of hybrid qubits is feasible.

*Gate fidelity.*—When hybrid qubits are not undergoing gate operations, their coherence properties benefit from their spin-like character, similar to singlet and triplet states in a two-electron quantum dot [26]. However, the gating procedures described above consist of sequential rotations of charge qubits, for which the decoherence rates are faster. The gating speeds are also faster, so realistic estimates for the gate fidelity require us to perform dynamical simulations of the gate sequence.

We model the dynamical evolution of the density matrix  $\rho$  using a master equation [21]:  $i\hbar\dot{\rho} = [H, \rho] + D$ . The Hamiltonian and decoherence terms are expressed in the  $\{|0\rangle_L, |1\rangle_L, |E\rangle\}$  basis as

$$H = \begin{pmatrix} 0 & 0 & t_1 \\ 0 & E_{01} & -t_2 \\ t_1 & -t_2 & -\varepsilon \end{pmatrix} \quad \text{and} \quad \frac{iD}{\hbar} = \begin{pmatrix} 0 & \gamma\rho_{01} & \Gamma\rho_{0E} \\ \gamma\rho_{10} & 0 & \Gamma\rho_{1E} \\ \Gamma\rho_{E0} & \Gamma\rho_{E1} & 0 \end{pmatrix}.$$

In  $H$ ,  $E_{01} \approx 0.1$  meV is the energy splitting between the logical qubit states [22], and  $t_1$  and  $t_2$  are the tunnel couplings. For valley-type excited states in Si,  $t_2 = \sqrt{3/2}t_1$  [22]. The charge dephasing rate [27]  $\Gamma = 1/T_2^* \approx 0.2$  GHz is the

experimentally measured value for charge qubits in GaAs [15], and the spin dephasing rate  $\gamma \approx 1$  MHz is the theoretical estimate for  $1/T_2^*$  of the hybrid qubit far from the anticrossings [26].

Figure 2 shows the results of our dynamical simulation for an  $X$ -gate (a  $\pi$  rotation around the logical  $x$  axis), using the gate sequence  $U = P_2BA(\pi)BP_1$  [24]. Increasing the tunnel coupling improves the fidelity because it increases the gate speed, until the  $A$  and  $B$  anticrossings overlap and the fidelity flattens out. The frequency at which this occurs increases as  $E_{01}$  increases.

Figure 2 also shows analogous fidelity calculations for the exchange gate that implements  $X$  rotations of singlet-triplet qubits [16,20] by pulsing to a value of  $\varepsilon$  at which the exchange coupling  $J$  dominates over the interdot magnetic field difference  $\Delta B$  [16]. There are competing effects in the fidelity when  $J \gg \Delta B$  (i.e., when  $|\varepsilon|$  is small): the qubit becomes chargelike, and decoheres more quickly, but the gate speed increases. In Fig. 2, the value of  $\varepsilon$  is chosen to yield the optimum fidelity for every  $\Delta B$  and  $t_1$ . Figure 2 shows results for three physical systems: GaAs ( $\gamma = 1/T_2^* = 0.14$  GHz,  $\Delta B = 3.6$  mT [28]), natural Si ( $\gamma = 1.5$  MHz,  $\Delta B = 26$   $\mu$ T [28]), and isotopically purified Si ( $\gamma = 0.2$  MHz,  $\Delta B = 1.2$   $\mu$ T [28]). For fixed tunnel coupling, increasing  $\Delta B$  reduces the fidelity of the exchange gate. However, better fidelities can be achieved by increasing  $\Delta B$  and  $t_1$  simultaneously.

Figure 2 shows that for natural silicon, the fidelity of an  $X$  gate in a hybrid qubit is comparable to the fidelity of an exchange-mediated gate (with  $J \gg \Delta B$ ) in a singlet-triplet qubit. The fidelity of a  $Z$  gate in a hybrid qubit is very high

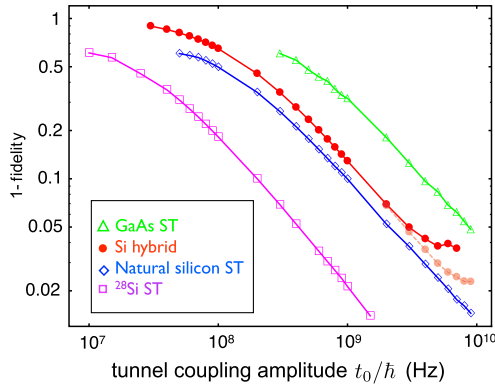


FIG. 2 (color online). Numerically calculated infidelity (1-fidelity) caused by dephasing during qubit rotations without use of dynamical decoupling [35], as a function of the interdot tunnel coupling in a double quantum dot. Solid red circles show the results for a hybrid qubit, and open triangles, diamonds, and squares show the results for the exchange gate of singlet-triplet (ST) qubits [16,20] for GaAs, natural Si and isotopically purified Si, with  $^{28}\text{Si}$  exhibiting the best overall gate fidelity. The two curves for the Si hybrid qubit represent different values of the singlet-triplet splitting (0.05 meV for the upper curve and 0.5 meV for the lower curve).

because it is a fast gate that is implemented far from any level crossings [22]. For a singlet-triplet qubit, the corresponding gate (with  $\Delta B \gg J$ ) is also implemented away from level crossings, but inhomogeneous broadening places a materials-dependent lower bound on the fidelity [28]. Fast pulse sequences can be used to overcome this constraint [29] at the cost of gating complexity. Hybrid qubit gates are simple for both rotation axes since they do not require complicated gating sequences.

Pulse-gated quantum operation can also be performed by combining slow ramps and fast pulses to perform adiabatic passage through the  $B$  anticrossing between  $|E\rangle$  and  $|1\rangle_L$  [30] and quantum oscillations at the anticrossing  $A$  between  $|0\rangle_L$  and  $|E\rangle$ . Starting from a large negative detuning, first the detuning is increased adiabatically through anticrossing  $B$  (which transforms  $|1\rangle_L \rightarrow |E\rangle$  and has no effect on  $|0\rangle_L$ ), then pulsed suddenly to anticrossing  $A$  (inducing quantum oscillations between  $|0\rangle_L$  and  $|E\rangle$ ), and finally decreased adiabatically through anticrossing  $B$  (which transforms  $|E\rangle \rightarrow |1\rangle_L$  and has no effect on  $|0\rangle_L$ ). This partially adiabatic protocol could be very useful if the energy splitting at anticrossing  $B$  is significantly larger than for anticrossing  $A$ , which is conceivable because of the large differences of tunnel rates from different orbital states that have been observed in a silicon quantum dot [31]. However, the time spent in  $|E\rangle$  is likely to be longer than in the all-sudden protocol described above, rendering the gate much more susceptible to charge noise, because of the markedly different charge distribution in  $|E\rangle$  than in  $|0\rangle_L$  and  $|1\rangle_L$  [26]. Thus it is likely to be more difficult to perform high-fidelity gate operations using a partially adiabatic process than using the sequence of quantum oscillations described above.

*Two-qubit gates.*—Two-hybrid qubit gates can be implemented by exploiting capacitive coupling [19,32,33]. As shown in Fig. 3(a), the charge distribution in state  $|E\rangle$  is substantially different than in  $|0\rangle_L$ , so there is a substantial Coulomb coupling that causes the location of the anticrossings  $A$  and  $B$  of the target qubit to depend on whether the control qubit is in state  $|0\rangle_L$  or in state  $|E\rangle$ . Therefore, pulsing the target qubit to the detuning of anticrossing  $A$  converts the state  $|1\rangle_L$  of the target qubit to  $|E\rangle$  when the control qubit is in state  $|0\rangle_L$  but not in state  $|E\rangle$ . This dependence of the position of the anticrossings of the target qubit on the state of the control qubit enables the construction of a conditional two-qubit gate, as illustrated in Fig. 3(c). One first applies a  $B$  gate to the control qubit, which transforms  $|1\rangle_L \rightarrow |E\rangle$ , and then applies a gate sequence that changes the phase of the target qubit only if the control qubit is in state  $|0\rangle_L$ . 2D Thomas-Fermi modeling [34] of the realistic device geometry shown in Fig. 3(b) and described in Ref. [24] yields shifts in the anticrossing energies of  $\approx 0.1$  meV, which is ample for fast operations to be feasible.

*Summary.*—We have presented a method for pulse gating a quantum-dot hybrid qubit. Even though the qubit states typically cannot be made energetically degenerate,



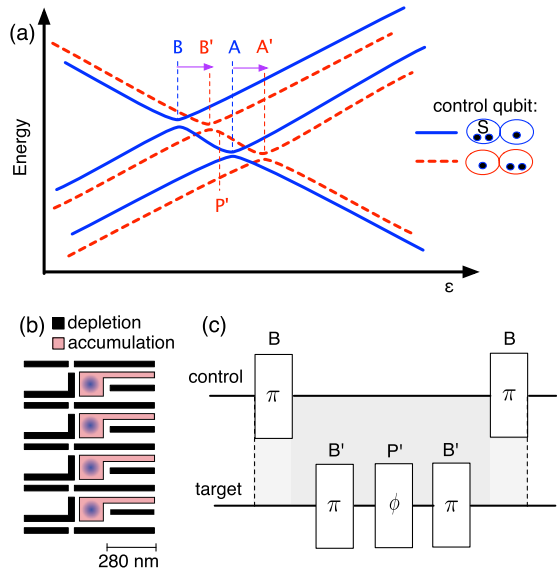


FIG. 3 (color online). Pulse-gating protocol for a two-qubit controlled-phase gate. (a) The detunings of the avoided crossings  $A$  and  $B$  of the target qubit shift by  $\delta\epsilon$  (horizontal arrows on the figure) when the state of the control qubit is changed from  $|0\rangle_L$  to  $|E\rangle$ . (b) Realistic device geometry for a top-gated Si/SiGe heterostructure, described in Ref. [24]. 2D Thomas-Fermi modeling [34] of this device yields  $\delta\epsilon \geq 0.1$  meV, ample for operation of a conditional gate. (c) Gate sequence for a conditional rotation of the phase of the target qubit. First, a  $B$  gate is applied to the control qubit, which leaves  $|0\rangle_L$  unchanged and transforms  $|1\rangle_L \rightarrow |E\rangle$ . The target qubit is then pulsed to anticrossing  $B'$ , then to  $P'$ , and then again to  $B'$ , which changes the phase of the target qubit only when it starts in state  $|1\rangle_L$  and the control qubit is in state  $|E\rangle$ . Finally, applying a  $B$  gate to the control qubit converts it back to a spin qubit. The gray shading denotes that the operations on the target qubit are conditional between application of the two  $B$  gates to the control qubit. This gate sequence changes the phase of the target qubit only when the control qubit starts in state  $|1\rangle_L$ . The operations also perform a conditional phase rotation on the control qubit, which can be adjusted to be a multiple of  $2\pi$  by appropriate choice of pulse parameters.

pulsed gating can be implemented by exploiting avoided crossings at two different detunings between each of the two qubit states and an intermediate state. With an additional phase gate at a third detuning, arbitrary rotations of the logical qubit can be achieved. We have derived explicit expressions for the pulse sequences and performed dynamical simulations of the gates assuming realistic values for the dephasing rates. We also showed that two-qubit gates can be implemented by operating the control qubit in the charge regime to electrically enable or disable a rotation on the target qubit.

We thank Xuedong Hu, Jon Prance, and Zhan Shi for useful conversations. This work was supported in part by ARO (Grants No. W911NF-08-1-0482 and No. W911NF-12-1-0607) and NSF (Grants No. DMR-0805045, No. PHY-1104660, and No. DGE-0718123).

- [1] D. DiVincenzo, *Science* **270**, 255 (1995).
- [2] J. Preskill, *Proc. R. Soc. A* **454**, 469 (1998).
- [3] A. Fisher, *Phil. Trans. R. Soc. A* **361**, 1441 (2003).
- [4] Z. Shi, C. B. Simmons, J. R. Prance, J. K. Gamble, T. S. Koh, Y.-P. Shim, X. Hu, D. E. Savage, M. G. Lagally, M. A. Eriksson, M. Friesen, and S. N. Coppersmith, *Phys. Rev. Lett.* **108**, 140503 (2012).
- [5] Z. Shi, C. B. Simmons, D. R. Ward, J. R. Prance, T. S. Koh, J. K. Gamble, X. Wu, D. E. Savage, M. G. Lagally, M. Friesen, S. N. Coppersmith, and M. A. Eriksson, *arXiv:1208.0519*.
- [6] F. H. L. Koppens, C. Buizert, K. J. Tielrooij, I. T. Vink, K. C. Nowack, T. Meunier, L. P. Kouwenhoven, and L. M. K. Vandersypen, *Nature (London)* **442**, 766 (2006).
- [7] J. Levy, *Phys. Rev. Lett.* **89**, 147902 (2002).
- [8] D. P. DiVincenzo, D. Bacon, J. Kempe, G. Burkard, and K. B. Whaley, *Nature (London)* **408**, 339 (2000).
- [9] J. M. Martinis, S. Nam, J. Aumentado, and C. Urbina, *Phys. Rev. Lett.* **89**, 117901 (2002).
- [10] M. Pioro-Ladrière, T. Obata, Y. Tokura, Y.-S. Shin, T. Kubo, K. Yoshida, T. Taniyama, and S. Tarucha, *Nat. Phys.* **4**, 776 (2008).
- [11] T. Hayashi, T. Fujisawa, H. D. Cheong, Y. H. Jeong, and Y. Hirayama, *Phys. Rev. Lett.* **91**, 226804 (2003).
- [12] J. Gorman, D. G. Hasko, and D. A. Williams, *Phys. Rev. Lett.* **95**, 090502 (2005).
- [13] J. R. Petta, A. C. Johnson, J. M. Taylor, A. Yacoby, M. D. Lukin, C. M. Marcus, M. P. Hanson, and A. C. Gossard, *Physica (Amsterdam)* **34E**, 42 (2006).
- [14] G. Shinkai, T. Hayashi, T. Ota, and T. Fujisawa, *Phys. Rev. Lett.* **103**, 056802 (2009).
- [15] K. D. Petersson, J. R. Petta, H. Lu, and A. C. Gossard, *Phys. Rev. Lett.* **105**, 246804 (2010).
- [16] J. R. Petta, A. C. Johnson, J. M. Taylor, E. A. Laird, A. Yacoby, M. D. Lukin, C. M. Marcus, M. P. Hanson, and A. C. Gossard, *Science* **309**, 2180 (2005).
- [17] E. A. Laird, J. M. Taylor, D. P. DiVincenzo, C. M. Marcus, M. P. Hanson, and A. C. Gossard, *Phys. Rev. B* **82**, 075403 (2010).
- [18] L. Gaudreau, G. Granger, A. Kam, G. C. Aers, S. A. Studenikin, P. Zawadzki, M. Pioro-Ladrière, Z. R. Wasilewski, and A. S. Sachrajda, *Nat. Phys.* **8**, 54 (2011).
- [19] M. D. Shulman, O. E. Dial, S. P. Harvey, H. Bluhm, V. Umansky, and A. Yacoby, *Science* **336**, 202 (2012).
- [20] B. M. Maune, M. G. Borselli, B. Huang, T. D. Ladd, P. W. Deelman, K. S. Holabird, A. A. Kiselev, I. Alvarado-Rodriguez, R. S. Ross, A. E. Schmitz, M. Sokolich, C. A. Watson, M. F. Gyure, and A. T. Hunter, *Nature (London)* **481**, 344 (2012).
- [21] M. A. Nielsen and I. L. Chuang, *Quantum Computation and Quantum Information* (Cambridge University Press, New York, 2000).
- [22] Z. Shi, C. B. Simmons, J. Prance, J. K. Gamble, M. Friesen, D. E. Savage, M. G. Lagally, S. N. Coppersmith, and M. A. Eriksson, *Appl. Phys. Lett.* **99**, 233108 (2011).
- [23] A  $\pi$  pulse at  $\epsilon_A$  also enables fast spin-to-charge conversion for readout, since it changes the charge state of  $|0\rangle_L$  but not  $|1\rangle_L$ .
- [24] See Supplemental Material at <http://link.aps.org/supplemental/10.1103/PhysRevLett.109.250503> for details of the calculations.

- [25] J. R. Petta, A. C. Johnson, C. M. Marcus, M. P. Hanson, and A. C. Gossard, *Phys. Rev. Lett.* **93**, 186802 (2004).
- [26] J. K. Gamble, M. Friesen, S. N. Coppersmith, and X. Hu, *Phys. Rev. B* **86**, 035302 (2012).
- [27] S. D. Barrett and C. H. W. Barnes, *Phys. Rev. B* **66**, 125318 (2002).
- [28] L. V. C. Assali, H. M. Petrilli, R. B. Capaz, B. Koiller, X. Hu, and S. Das Sarma, *Phys. Rev. B* **83**, 165301 (2011).
- [29] H. Bluhm, S. Foletti, I. Neder, M. Rudner, D. Mahalu, V. Umansky, and A. Yacoby, *Nat. Phys.* **7**, 109 (2011).
- [30] Y. Nakamura, *Nonadiabatic Transition: Concepts, Basic Theories and Applications* (World Scientific, London, 2001).
- [31] C. B. Simmons, J. R. Prance, B. J. Van Bael, T. S. Koh, Z. Shi, D. E. Savage, M. G. Lagally, R. Joynt, M. Friesen, S. N. Coppersmith, and M. A. Eriksson, *Phys. Rev. Lett.* **106**, 156804 (2011).
- [32] T. Yamamoto, Y. A. Pashkin, O. Astafiev, Y. Nakamura, and J. S. Tsai, *Nature (London)* **425**, 941 (2003).
- [33] I. van Weperen, B. D. Armstrong, E. A. Laird, J. Medford, C. M. Marcus, M. P. Hanson, and A. C. Gossard, *Phys. Rev. Lett.* **107**, 030506 (2011).
- [34] M. Stopa, *Phys. Rev. B* **54**, 13767 (1996).
- [35] L. Viola, E. Knill, and S. Lloyd, *Phys. Rev. Lett.* **82**, 2417 (1999).